Impact of PIP2 Lipids, Force Field Parameters, and Mutational Analysis on the Binding of Osh4's α_6-α_7 Domain

Robert J. Allsopp[1] and Jeffery B. Klauda[1,2,*]
[1]Department of Chemical and Biomolecular Engineering
[2]Biophysics Graduate Program
University of Maryland, College Park, MD 20742, USA
*Corresponding Author: jbklauda@umd.edu

Abstract:

All atom molecular dynamics (MD) simulations are used with the Highly Mobile Membrane Mimetic (HMMM) method to study the α_6-α_7 peptide of the critical yeast Osh4 peripheral membrane protein. This research focuses on the impact of phosphatidylinositol-4,5-bisphosphate (PIP2) lipids and 1-palmitoyl-2-oleoyl-*sn*-glycero-3-phospho-L-serine (POPS) on the protein's ability to bind to the membrane. Details of the binding mechanism are described qualitatively and quantitatively by measuring the position of the deepest residues, angle of the peptide during binding, root mean square deviation (RMSD) of the atomic positions within the peptide, and interaction energy, while changing variables, such as the force field used and the presence of the PIP2 lipids. The negatively-charged PIP2 has a large headgroup that is a few Ångstroms above the main membrane phosphates enabling the PIP2 lipids to interact with the peptide before it binds deeper into the membrane. The PIP2 lipids can alter the position of the peptide during binding by recruiting charged residues on the α_7 helix, such as R344 and R347. Residues R347 and R344 are unusual because they are slightly out of the reach of the main membrane phosphates, but optimally positioned to interact with the PIP2 lipids. The salt bridge interactions can also typically occur between cationic peptide residues such as R314, K325, and K336. The force field interactions effect on peptide binding was also investigated by changing the standard CHARMM36m to an improved description between some amino acids and lipid moieties (*Phys. Chem. Chem. Phys*. **20**: 8432-8449). This resulted in the total number of salt bridges and hydrogen bonds being drastically reduced, the interaction energy was also reduced, and there was more balance between electrostatic and non-polar interactions, but the general bound structure is maintained. This work is an important initial step to understanding the effect of the Osh4 protein on the membrane binding and to quantify the effect of PIP2 lipids on this domain.

Introduction:

Since all cells have lipid membranes, it is crucial to understand the role of lipid transport proteins to maintain membrane composition. Lipid transport involves the mechanism of transporting lipids between and within different cellular membranes, and is usually studied in model eukaryotic cells such as yeast.[1] Since lipid transport proteins are in control of modulating the lipid composition of membranes, they also regulate many cellular processes including vesicular trafficking, signal transduction, and lipid metabolism.[1-4] Lipid trafficking is controlled by several different transporters, in addition, lipid transport can be observed between organelles that are not connected to vesicular transport machinery such as the mitochondria and peroxisomes; and proves that non-vesicular lipid transport plays an important role in the total lipid transport.[1, 5, 6] Finally, there is evidence that intracellular lipid transport is enhanced at membrane contact sites, which are small gaps of 10-20 nm that form between organelles.[1, 7-9]

Intracellular membrane composition is partially controlled in yeast, by a family of seven Oxysterol-Binding Homology (Osh) proteins that have overlapping roles.[10] Although the Osh family of proteins are specific to yeast, there are homologous proteins in mammals.[10] A key feature is that each of the proteins has an affinity for a certain membrane compositions and thus organelles.[11] Osh4 localizes to the endoplasmic reticulum[12] and Golgi complex,[10] while the plasma membrane is associated with Osh2, Osh6, and Osh7.[11] The Osh family consists of seven total proteins with the first three (Osh1-Osh3) being significantly longer in sequence (>1100 residues) compared to the Osh4-7 proteins which are smaller (~430 residues). Osh1-3 binding studies include the phosphatidylinositol (PI) binding pleckstrin homology (PH) domains[13] with Osh1's PH domain selective for lipids in the Golgi.[14] All Osh proteins have an oxysterol binding domain, which also has affinity for lipids with two phosphates, such as the one studied here 1-palmitoyl-2-

oleoyl-*sn*-glycero-phosphoinositide 4,5-bisphosphate (PIP2).[11] This domain is where lipids and sterols are held as they shuttle between organelles during the lipid transfer process.

The focus of this work is on one of the lipid transport proteins in yeast, i.e., Osh4. This protein is composed of multiple domains that are involved in the membrane binding mechanism and protein function. The Oxysterol Binding Protein Related Domain (ORD, grey in Figure 1) is responsible for uptake and placement of the lipids that are transported and is conserved among all Osh proteins.[11] Another common domain is the amphipathic lipid packing sensor (ALPS, blue in Figure 1),[10] which is known to be important to binding and senses curvature or lipid packing due to its amphipathic structure.[15]

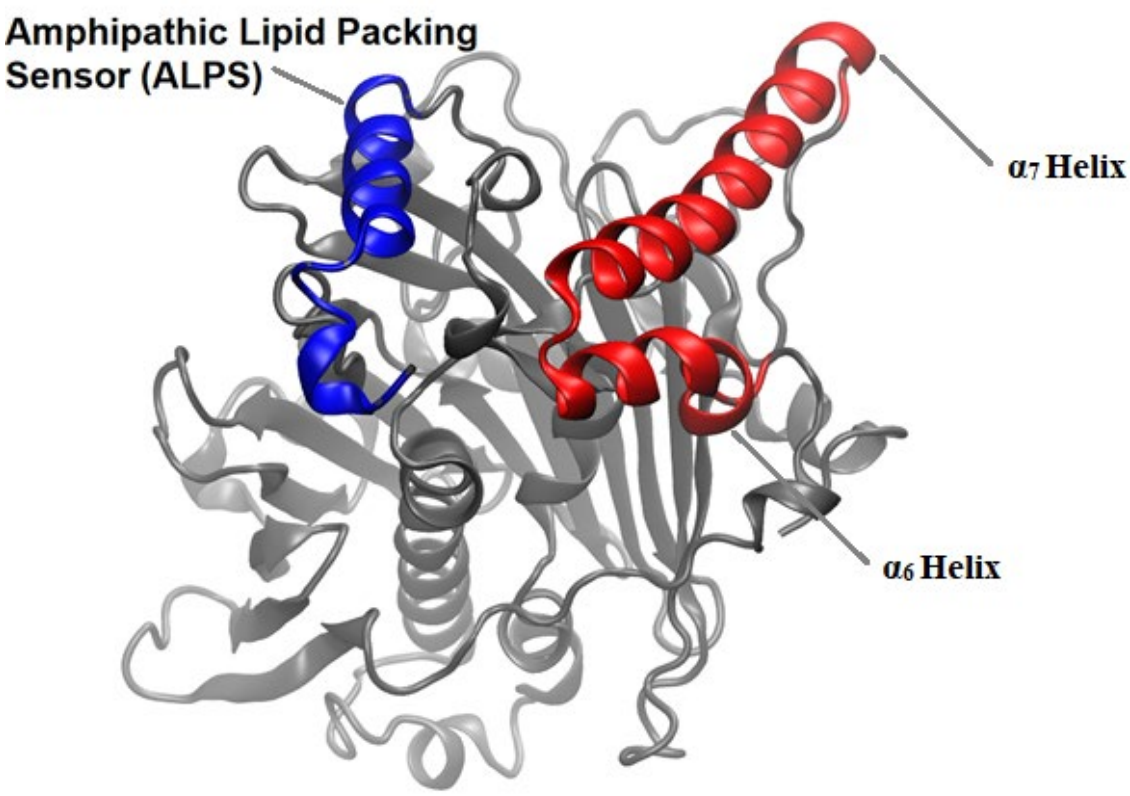

Figure 1. This image shows the ALPS (blue) and α_6-α_7 helix (red) in relation to the entire Osh4 protein (silver).

The binding region in question for our work ranges from residues E312 on α_6 to I355 on α_7 (red in Figure 1). It is unknown if the α_6-α_7 domain independently interacts with the membrane, but there is evidence showing these residues play a key role in the function of the protein, and the objective of this research was to further investigate these interactions. First, from the location of this domain in the crystal structure, the α_6-α_7 domain is far away from the lipid transport section of the protein, so that loss of function is not necessarily related to a loss of ability to extract PI4P.[10] K336 was found to be essential,[10, 16] because binding affinity and labeled cholesterol transference of Osh4 was considerably reduced when K336 was mutated to non-polar alanine. Moreover, the E312K mutant resulted in a loss of function.[17] In the original article that published Osh4's structure, sulphate ions bound to K336 and potentially mimic the role of membrane phospholipid phosphates.[10] It is also noted that the region surrounding E312K lies within a domain that exhibits features of a Pleckstrin homology (PH) domain, which is a known domain that binds to PIP lipids.[17]

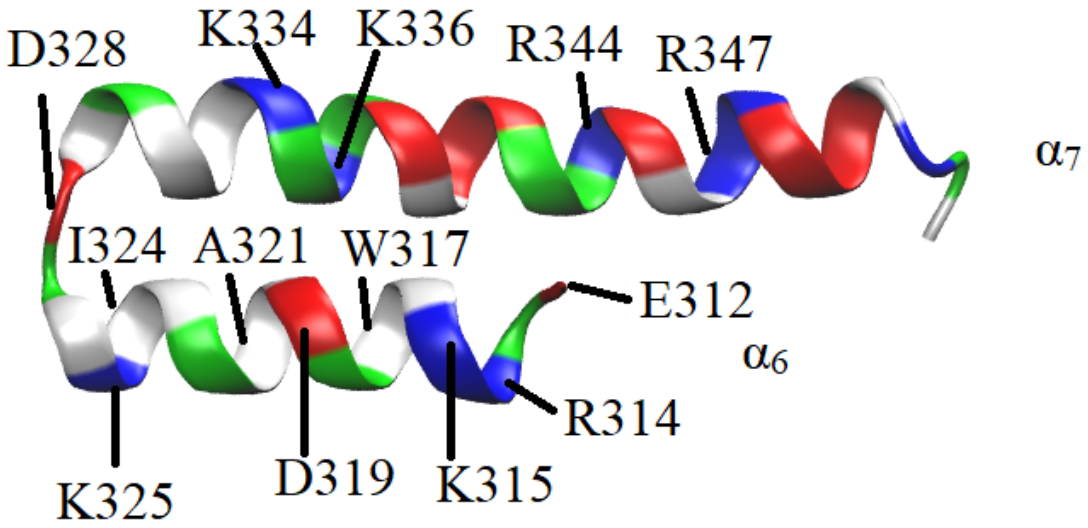

Figure 2. The α_6-α_7 peptide is oriented so that the facing residues, K334, K315, D319 and E312 tend to have less interaction with the membrane while the inward residues, K325, R314, D328

interact nearest to the membrane. Red coloring is negatively charged, blue coloring is positively charged, white is hydrophobic, and green is polar. The helices also have non-polar residues on the opposite side of the polar face. For the α_7 helix, the main amino acid residue interacting with the membrane is K336. However, there are additional residues such as R347 and R344 that hover above the membrane but still interact with the membrane and this is consistent with the simulations.

While there are other domains on Osh4 that interact with the membrane, it was decided to limit the scope in this research to the α_6-α_7 helices before considering the more complicated full protein. This research serves as a test if this domain can bind to model membranes. We investigated the effect of membranes having a mixture of 1-palmitoyl-2-oleoyl-glycero-3-phosphocholine (POPC) and 1-palmitoyl-2-oleoyl-glycero-3-phosphidylserine (POPS) lipids and the presence of a few PIP2 lipids. Functionally Osh4 extracts PI4P from membranes but was not considered here as the α_6-α_7 helical domain is away from the PI4P binding pocket.[18] It is known that PIP2 lipids are not needed for binding, however, PIP2 is speculated to assist the binding process by increasing the dwell time of the peptide on the liposome surface,[13, 17] which is why this lipid was included in our study. Some of the amino acids that are hydrophobic and are likely attracted to the membrane include I324, A321, and W317. Simulations will be used to determine which residues of the peptide drive the binding process, and the orientation of the bound peptide before and after binding.

Four *hypotheses* that were probed in this work include: *1*. Certain residues play a key role in the binding process, *2*. The mechanism of peptide binding is related to the angle of helical approach, 3. Peptide bound orientation differs in membranes with and without PIP2, and *4*. Salt-bridge interactions between the two helices stabilize the membrane binding structure.

This report is organized into a Methods Section, then Results and Discussion, and finally, the Conclusion. The Methods Section explains how the simulations were setup and details needed to reproduce the work. Specifically, this section describes two lipid compositions, initial builds for equilibration, simulation conditions, and how different analysis were performed. The Results and Discussion Section discusses PIP2 and non-PIP2 binding parameters, including binding mechanisms, force field dependence, structure of peptide and placement in the membrane, the residue-membrane interactions important to binding, PIP2-specific interactions, and mutational analysis to understand the binding process.

Methods:

Molecular dynamics simulations were used to study the Osh4 α_6 and α_7 helices interacting with membranes of POPC, POPS, and PIP2. The MD simulations were divided into two sets, one with PIP2 lipids and the other without. The simulations without the PIP2 lipids were composed of 40 POPC and 10 POPS in bilayers of 50 lipids per leaflet (80% POPC and 20% POPS). The simulations with PIP2 lipids were composed of 40 POPC, 10 POPS, and 3 PIP2 in bilayers of 53 lipids per leaflet, where the lipids were evenly distributed between the two leaflets (75.4% POPC, 18.9% POPS, and 5.7% PIP2). Although the simulation box was relatively small it was sufficient for this research since there were no interactions between the primary space peptide and its image.

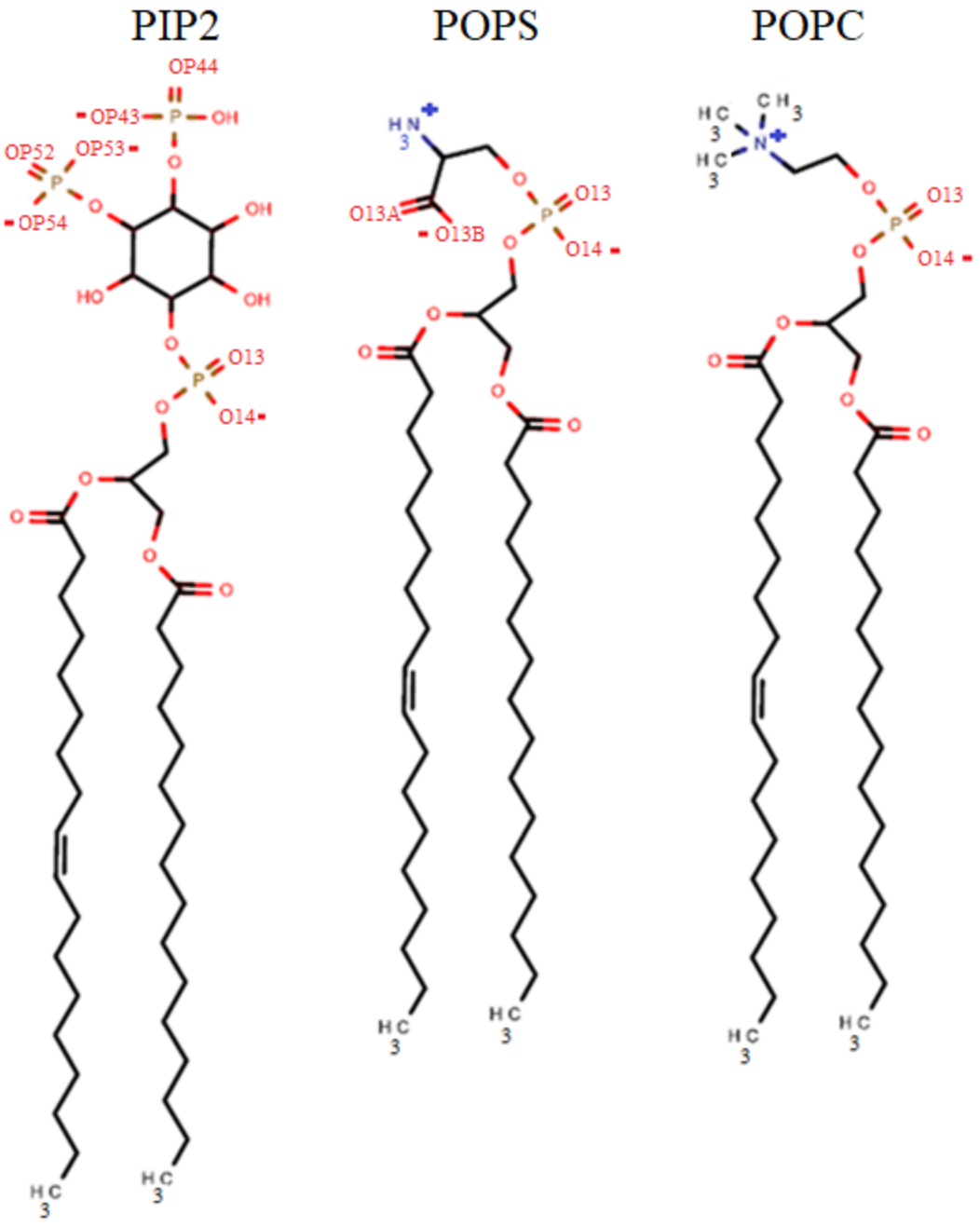

Figure 3: This is an image of the three lipid types that were used in the simulations 1-palmitoyl-2-oleoyl-*sn*-glycero-phosphoinositide 4,5-bisphosphate (PIP2), 1-palmitoyl-2-oleoyl-*sn*-glycero-3-phospho-L-serine (POPS), and 1-palmitoyl-2-oleoyl-glycero-3-phosphocholine (POPC). The images were created using Marvin for drawing the chemical structures.[19]

The membrane models were built with the HMMM builder feature within the *Membrane Builder* of CHARMM-GUI (www.charmm-gui.org)[20-26] with either 83 or 120 molecules of water per lipid for either the horizontal or vertical orientations using the TIP3P model[27] for water, and neutralizing potassium ions were added to the mixture. The HMMM builder feature accelerates the simulation with a simplified approach by modeling only the individual lipid head groups and replacing the tails with DCLE solvent without the extended lipid tails allowing for an increase in lipid diffusion.[23] It is known that the HMMM model accelerates the diffusion of the lipids by an order of magnitude, without affecting the mechanism of attachment, thereby saving computational resources without losing details of binding.[23, 28] Each of the models was equilibrated using the standard six-step CHARMM-GUI[21, 22] protocol for 225 ps. To simulate the α_6-α_7 helix, the peptide coordinates that range from E312 to I355 were extracted from the full protein (PDBID: 1zhy[10]) and the terminal group was patched with the charged NTER and CTER patch without acetylation or methylation. The NTER and CTER capping method was used based on a review of initial results of simulations that did not identify any adverse interactions of significance with these charged terminal residues. Next, the peptide was inserted into the aqueous phase with different orientations and distances away from the membrane in CHARMM-GUI without forcing major peptide-membrane interaction and equilibrated for 225 ps before it was prepared to run with Nanoscale Molecular Dynamics (NAMD),[29, 30] by completing the six standard CHARMM-GUI equilibration runs that also used NAMD and the process involved minimizing the system and then simulating it with decreasing levels of restraints. The lipid area scaling factor was set to 1.3 with a terminal acyl carbon *number* of 6.[23] These settings help accelerate the binding process by exposing the lipid tails to the solvent and allowing for increased packing defects in the membrane.[23] The equilibration and

production runs ran with a 2 fs time step. Other settings for the equilibration include a restart frequency of 500 steps, a trajectory and extended system output frequency of 1000 steps. The frequency for all was changed to 5000 steps for the production runs. All of these initial equilibration and production runs used NAMD on a constant Number, Pressure, Area, and Temperature (NPAT) ensemble for approximately 150-200 ns of total simulation time.[29, 30] All simulations used the SHAKE algorithm to constrain hydrogen atoms.[31] Each membrane system has ten replicates that have five unique initial peptide orientations (horizontal (H) and vertical (V)) with details in Table S1. For these five initial placements, two replicas are simulated (10 total) to provide better sampling of the binding to model membranes. For all simulations, the CHARMM36 (C36) lipid force field[32] was used since it has the most updated parameters for the PIP lipids.[33] The C36m additive all atom protein force field was used[34, 35] and the TIP3P water model.[27, 34] Finally, the force field was changed after 150 ns of full-lipid simulation to the CUFIX parameters,[36] which was run for an additional 150 ns with an adjustment in the strength of ionic interactions so that the results of this work will be comparable with other ongoing research.

Van der Waals and electrostatic forces were computed using a Lennard-Jones force-switching function over 10 to 12 Å.[37] The temperature was kept constant at 303.15K to ensure a fluid phase membrane using the Nosé-Hoover thermostat and Langevin dynamics.[38] All simulations were run with periodic boundary conditions (PBC) that were used to evaluate long-range electrostatic interactions using the Particle Mesh Ewald (PME).[39]

Four of the HMMM simulations from each membrane model were chosen for conversion to full-length simulations via CHARMM-GUI *HMMM* to full-lipid converter and run again with NAMD for 150 additional ns. For the all-atom systems, temperature was held constant like the HMMM simulations but the box size varied semi-isotropically (X=Y but not Z) while keeping

pressure at a value of 1.01325 bar using a Langevin piston.[40-42] This allowed for the membrane to more closely resemble natural membrane lipid packing. The non-PIP2 simulations were chosen based on differences in orientation from the deepest residue graphs, and the PIP2 simulations were selected for depicting the full range of interactions between the PIP2 lipids and the peptide.

For the analysis of peptide binding to the membranes, the minimum penetration distance graphs were generated by measuring the vertical positions of all the peptide residues in VMD[43] around the binding region as well as the average phosphate position over every frame. This method was used for the minimum position graphs and the angle graphs. The figures were rendered with VMD Tachyon internal memory processing.[44] It was determined that the binding was impacted by two different angles, the angle of approach (θ) and the angle of rotation (ϕ) (Figure 4). The angle of approach (θ) measures the angle between the peptide and the membrane. The rolling angle is measured between residues I324 and N330, while the angle of approach is measured separately for each helix between residues K315 to L326 on the α_6 and residues N330 to K353 on the α_7.

A steep angle of approach (θ) means that the trailing ends of the helices are further away from the membrane. The angle of rotation (ϕ) determines whether the α_6 or the α_7 is closest to the membrane. A flat angle of rotation means that the α_6 and α_7 helices are at the same distance from the peptide, while a 90° rotation results in the α_7 above the α_6 helix. This orientation results in the α_6 helix closer to the membrane and is referred to as the peptide approaching the membrane on the side. This was calculated using the VMD orient package by defining the angles with several residues and then selecting only the z component and subtracting 90°.

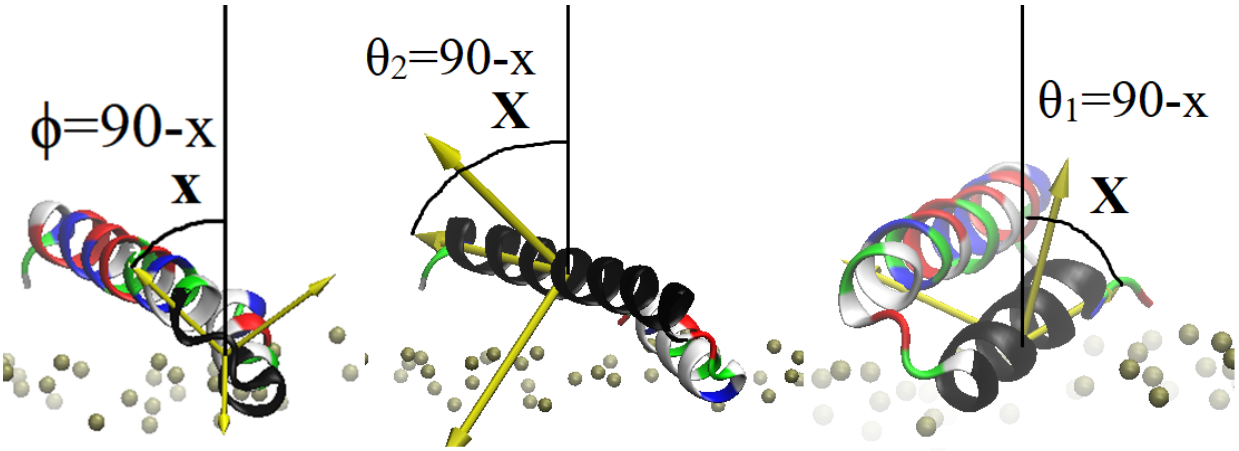

Figure 4. Left shows the ϕ angle, defined by the vector from residues I324 to N330 (black) and its angle with the bilayer normal, that measures the angle of rotation. The middle shows angle θ_2, defined by the vector of residues N330 to K353 (black) with the bilayer normal and measures the angle of approach of the α_7 helix, θ_1 is defined similarly except with residues K315 to L326 on the α_6 helix. The color scheme for the peptide are cationic (blue), anionic (red), non-polar (white), and polar (green).

The interaction energy (calculated with the CHARMM program) per residue is the sum of the van der Waals and the electrostatic contributions. The hydrogen bonds are based off a 3 Å cutoff and a 20° angle cutoff using the VMD Hbonds plugin. The distance used to calculate the hydrogen bond cutoff is defined as the distance from the heavy atom of the hydrogen bond acceptor to the hydrogen on the hydrogen bond donor. The angle is defined internally by VMD as an angle between the donor and acceptor atoms. The salt bridges between the peptide and the membrane were measured with CHARMM, and the CHARMM program counts more salt bridges than there are hydrogen bonds because there is no angle cut off. The salt bridges were calculated by using a hbonds function in CHARMM, but only salt bridge interactions were examined, no hydrogen bonds. The distance cutoff was set to 3Å for these peptide-membrane salt bridges differing from

the peptide-peptide salt bridge cutoff of 4 Å. There was no angle cutoff set, and the atoms that were being examined include resonance and the PIP specific atoms include OP43, OP44, OP52, OP53, OP54, along with O13, O14 which are the two resonance pairs shared among all of the lipids and lastly O13A and O13B that are on the POPS lipid. There were two positively charged atoms on the lipids that include POPS and POPC named N.

Results and Discussion:

This study evaluates the role of PIP2 lipids on the binding mechanism of the α_6- α_7 peptide and its fully-bound state to the membrane focusing on the PIP2 specific interactions, peptide structure, and residues critical to binding. The important residues that help orient the peptide before binding appear to be determined by a few charged lysine amino acids that are attracted to the membrane phosphates. Several parameters of the peptide binding are explored, such as, the peptide orientation during and after binding, the deepest residue center of mass (COM), the role the salt bridge plays in stabilizing the peptide, PIP2 sensitive conformational change, and the influence of binding with an updated force field. The binding interactions and energy were also evaluated to determine where the PIP2 lipids interact with the peptide. Replicas for these simulations are noted based on their initial configuration, i.e., H=horizontal and V=vertical, relative to the membrane surface. Five orientations were used (H1, H2, H3, V1 and V2) and duplicates of these were also simulated so H1a and H1b are the same starting point but varied trajectories.

Peptide Binding to non-PIP2 Lipid Membranes

Peptide Binding Mechanism to HMMM

The following section was included to gain insights into the binding mechanism which address *hypothesis 1* (the binding key residues) and *hypothesis 2* (the mechanism of peptide

binding). The simulations of peptide binding to HMMM were produced into movies and included in the Supporting Materials, such as *Movie 1* (H1a), *Movie 2* (H1b), *Movie 3* (H2b), *Movie 4* (H3a). These show the binding process and mechanism. Two different binding approaches were observed during the HMMM phase of the simulations, the first approach (50% of the time) was with the peptide on its side as it approached the membrane (Figure 5A); Figures S1-S2 show the position of the instantaneous deepest residue COM over time and was used to visualize the binding process. In the second approach, the peptide remains flat with both helices at the same level as the peptide approached the membrane (Figure 5B). An important residue that was identified is K325 that is positioned on the side allowing the peptide to interact with the lipid head groups as the peptide comes closer to the membrane especially during the side approach (Figure 6). K325 and R314 are the only charged residues on the otherwise relatively uncharged α_6 helix. As the non-polar residues lodge deep in the membrane, K325 is brought to a similar level as seen in Figure 6.

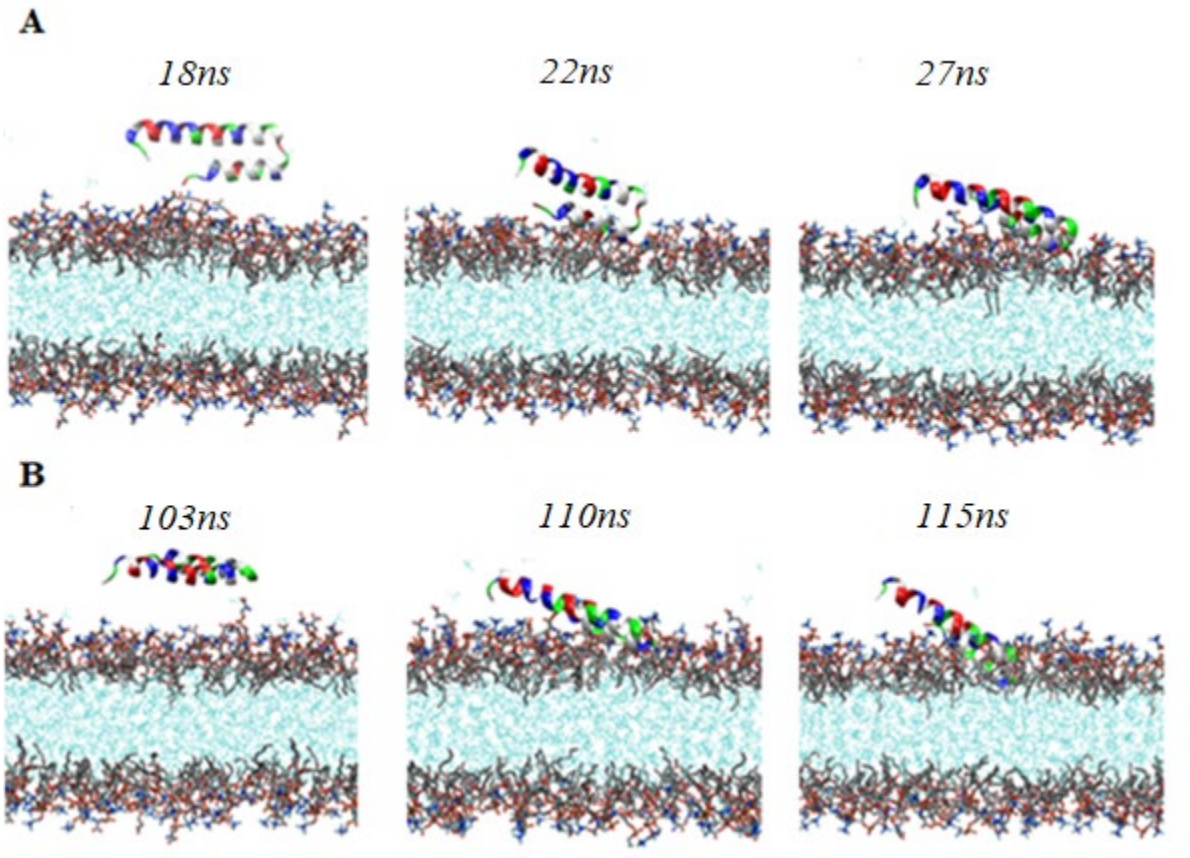

Figure 5: The binding approach for the rolling motion around the horizontal axis where the peptide transitions from a 90° angle of rotation ϕ (the longer α_7 helix is on top of the α_6 helix) to 0° (the two helices at the same level) (**A**) peptide rolls sideways in H1a, (**B**) peptide approaches flat and rotates to a less extreme ϕ angle in H3a. The hydrophobic DCLE core is shown a cyan with the short-tailed lipids in silver (carbon), red (oxygen), gold (phosphorous) and blue (nitrogen).

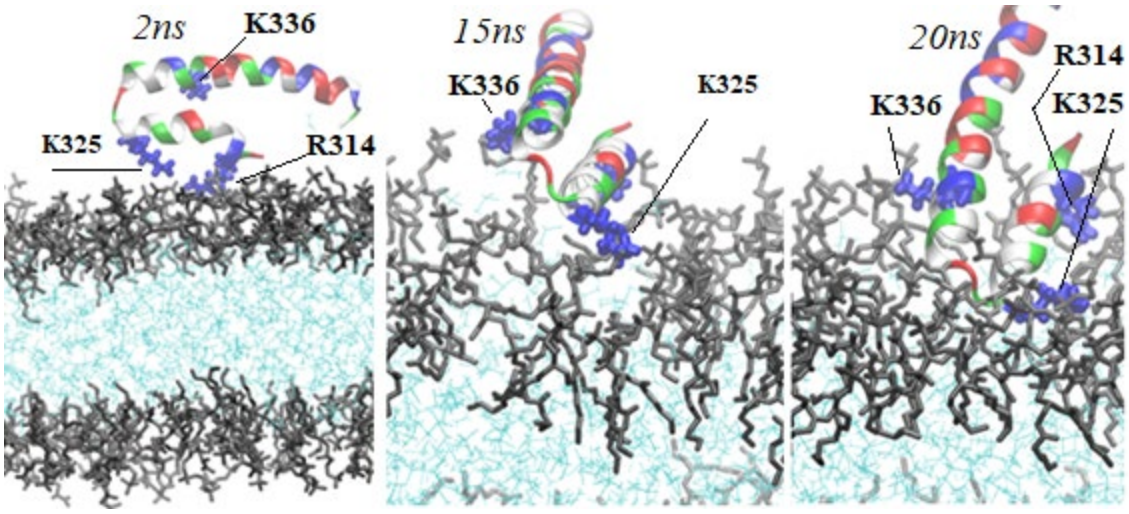

Figure 6: H1a showing the three key residues, R314, K325 on the α_6 helix, and K336 on the α_7 helix as the peptide approaches to bind onto a membrane in H1a. The hydrophobic DCLE core is shown as cyan with the short-tailed lipids in silver.

Due to equilibration and eventual binding process, the peptide's structure altered from the original crystallographic structure as is expected with MD simulations in a varied environment. The RMSD of the peptide was calculated to illustrate changes to the peptide structure over time (Figure S3-S4). Generally, the RMSD is 3-4 Å with an exception of the V2a replica due to deformation of the α_7 helix. This indicates that nearly all runs maintained most of the starting crystal structure as this RMSD range is typical for MD simulations.

Based on the simulations, three positively-charged residues (R314, K325, and K336) drive the binding process narrowing *hypothesis 1* to these three residues. These simulations further revealed that the passage of the peptide through the main phosphate layer was initiated by the lysine residues that make first contact due to electrostatic attraction to the phosphates.

Regarding *hypothesis 2*, the orientation of the peptide is measured to assess the impact on the binding process. The rolling motion of the peptide is measured by the angle of rotation ϕ in

Figure S5-S6, but nothing noteworthy was identified from this parameter other than the wide variation during binding. The angle of approach θ was measured individually for each helix during and after binding, which revealed that some simulations had high and low angles of approach after binding. Specifically, simulation H2a and H2b had the lowest angles of approach (Figure S7-S8) after binding. All of the measured angles can be seen in Figures S5-S10. Although the binding mechanism varied with these angles, there lacked a clear single mechanism of binding, thus our tested h*ypothesis 2* was shown to be invalid. Figures S11-S12 show the final bound states for the non-PIP2 HMMM simulations.

Structure of Peptide and its Placement in the Full-Membrane

The full-length lipid simulations were used to refine the HMMM bound state to better understand the membrane-binding states of this peptide with a total of four of the non-PIP2 simulations (H1a, H2a, H1b, and H2b) chosen. The decision to use these four simulations was based on differences in the HMMM results in the angles of approach and bound states. To analyze how the relative protein structure varies over time, the RMSD of the peptide was calculated for all the full-length simulations (Figures S13-S14). The final bound states of the two full-length simulations are shown in Figure 7, along with an image of the peptide with intra-peptide salt bridges.

In Figure 7A-D, there are several end snapshots taken from the simulations. The two different orientations refer to the high and low angle of approach. These images indicate that there are wide variations in the angle of approach θ_2, during the simulations and that there are different states accordingly. The high angle state (H1a and H2a) has an average θ_2 angle of 29.0° and the others have a low θ_2 angle is on average 14.4°. Although the results support *hypothesis 3* because

the orientation of the peptide can vary based on the angle of approach, additional study of the link to the PIP2 is needed and included later in this paper.

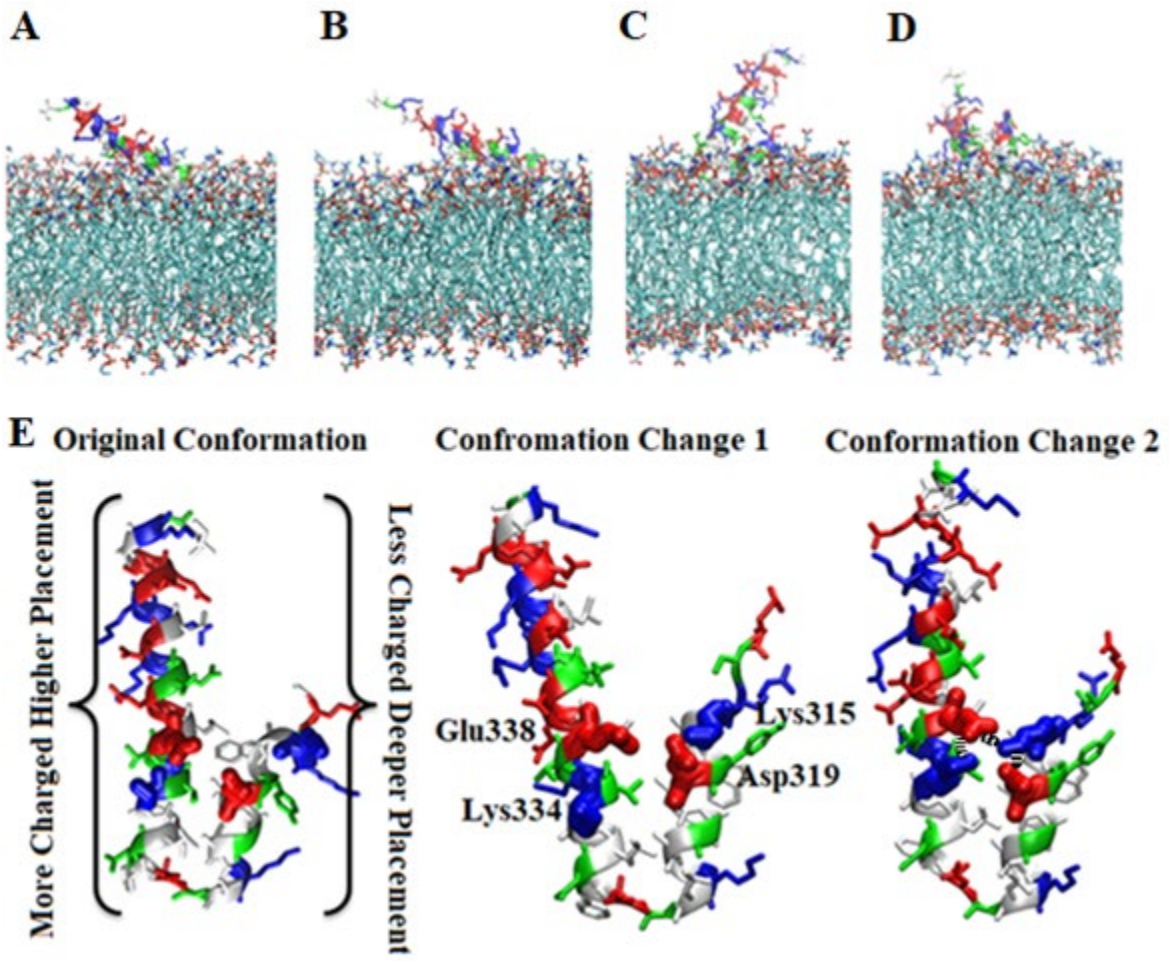

Figure 7: Images from full-length simulations **A**. is the final bound state of H1a **B**. is the final bound state of H2a, **C**. is nearly the final bound state of H1b, **D**. is nearly the final bound state of H2b. **E.** an image showing the structure of the peptide from H2a, with four electrostatic residues labeled to show that an intra-peptide salt bridge exists which helps stabilize this important region of the peptide. There was one simulation where the distances were close enough to be classified as salt bridges, H1a.

While *hypothesis 1* asserts that certain residues play a key role, other low energy residues exist that support the binding, but are less essential due to how they are placed in the membrane. The per residue interaction energies (Figure S15), the hydrogen bonds (Figure S16), and the salt bridges (Figure S17) are shown in the supporting materials. R314, K325, and K336 have elevated values for all three parameters and are thought to be crucial to the binding process by helping to bring the hydrophobic portion into the hydrocarbon region. On the other hand, R344 and R347 appear to be less essential because of their placement, meaning they do not reliably contact the membrane surface, as opposed to R314, K325, and K336 which are believed to help orient the peptide. The other residue that appears to be non-essential is K315 since it only has a high value of interaction in simulation H2a. Upon further examination, the increase in the interaction energy is believed to have resulted from a POPS lipid hydrogen bonding to the nitrogen backbone. Since there are only a few salt bridges with the charged portion of the peptide, but that there is a considerable number of hydrogen bonds.

Regarding *hypothesis 4*, the simulations were examined to correlate the salt bridge interactions with the stability the membrane binding structure. As mentioned above, there are a series of interactions range from direct peptide-peptide salt bridges (H1a) to no peptide-peptide interaction, but allow for interaction with lipids on the sides. The most observed conformation was the one in the middle of the bottom panel of Figure 7 with a slight rearrangement from the original structure. The conformation on the right was observed only once and that occurred in the H1a full length simulation but was sustained for about 120ns. This is the first spontaneous transition from a state of no interaction during the end of the HMMM, to a much closer conformation with a salt bridge between K315-E338, and finally to have it naturally break up. This confirms the validity of *hypothesis #4.* However, these peptide-peptide interactions are not essential for maintaining the

structure of the peptide since there were no drastic changes after the conformational change was broken up. The peptide-to-peptide salt bridges may promote folding in the aqueous phase by forming an attraction between the α_6-α_7 helices to form a side-by-side motif. The four amino acids involved in these potential salt bridges are specifically marked in Figure 7, i.e., K315, D319, K334, and E338. The distances between these amino acids versus time are shown for all the non-PIP2 simulations in Figures S19-S21. The ones that are believed to be close enough to be salt bridges have distances below 4 Å and are less frequently observed for K315-E338 which bridges between the α_6-α_7 helices. There is no indication of water-mediated interactions and the majority of the time there are either direct salt bridges or no interactions at all. The most stable simulation of all the non-PIP2 full-length simulations was H1a and had bridges during full length simulation less than 4 Å between D319-K315, 52% of the time, between K315-E338, 35% of the time, and between E338-K334, 16% of the time. All of the salt bridge occurrences for all runs can be found in the Table S3 and S4, based on residues close enough to qualify as salt bridges.

In terms of peptide placement, Figures S22-S25 show the relative position of each residue. In general, the α_6 helix fully contacts and most of it penetrates the membrane while only a portion of the α_7 helix is in full contact with the membrane, and most of it lies above the membrane. An interesting aspect of the peptide is that R347 and R344 approach close enough to hover around and interact with the lipid head groups. The placement graphs were also helpful for observing differences in the position of K315 to explain why some simulations had POPS lipids around K315 but did not interact with them. Specifically, for H1a and H2b, had lipids around K315 but did not interact with K315. The reason why the POPS lipids did not interact could be explained by the higher placement above the membrane as shown in the placement graphs. It is very intriguing that this residue that may specifically interact with POPS can vary greatly between simulations.

Peptide Binding to PIP2 Lipid Membranes

Peptide Binding Mechanism to HMMM

The HMMM simulations of the PIP2 simulations were also produced into movies in the Supporting Materials, i.e., *Movie 5* (V1b PIP2) and *Movie 6* (V2b PIP2), which feature the PIP2 lipids that are on either side of the peptide in V1b PIP2 and the peptide on top of the PIP2 lipids in V2b PIP2. In general, the peptide had the same tendency to orient to one of two main binding approaches. The major difference is that PIP2 lipids can interact electrostatically with residues on both helices before the peptide fully binds to the membrane. As seen in Figure 8A, the residues interact with the PIP2 lipids first before interacting with the other lipids. There are several other figures that feature the bound states of the peptide including Figures S26-S28.

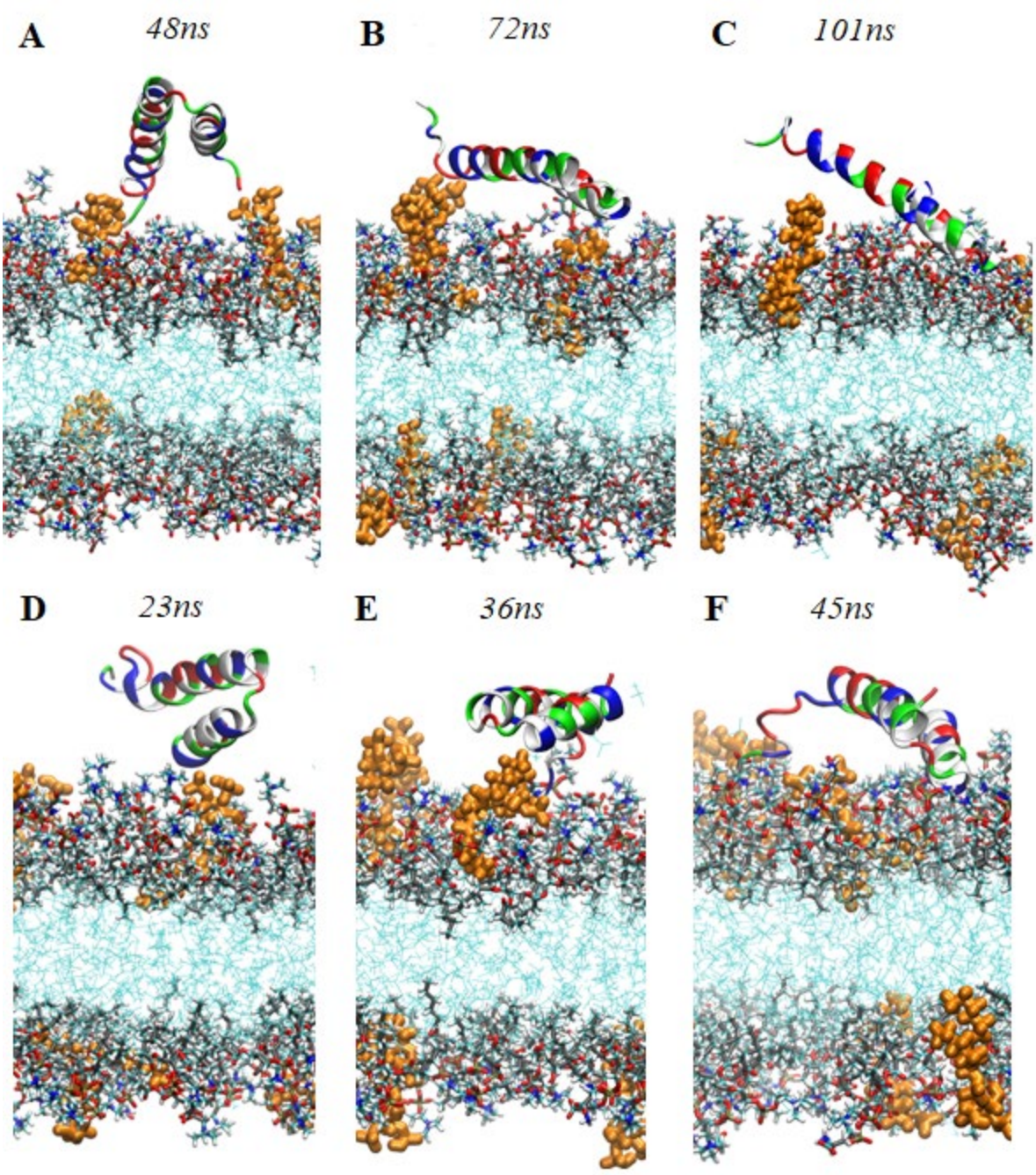

Figure 8: In these images the darker colored components represent the lipid heads, the light blue is DCLE, and the orange color is PIP lipids. Sequence of binding: (**A-C**), simulation H2a displays the result of PIP2 lipids recruiting the α_7 helix before binding and with positively charged residues

on the α_7 and α_6 helices. (**D-F**), simulation V1a, displays a PIP2 lipid that was once stabilizing K325 and is transitioning from the α_6 helix which is binding to the α_7.

Although the goal for the PIP2 lipid trials was to sample as many different orientations as possible that had peptide-PIP2 lipid interaction, only four stable states were observed with interactions close enough for PIP2 lipid interaction. These observed states with one replica each were run for an additional 150ns as full-tailed lipids and are shown in Figures S29 and S30.

Structure of Peptide and its Placement in Full-Membrane

The placement of the peptide in the membrane is much different in membranes with PIP2 lipids as these interact with the terminal ends the peptide (Figure 8A-C). This is illustrated in Figure S31 where the deepest residues are around I324-K325 and the higher residue numbering steadily increase in distance from membrane. Not all simulations have PIP2 lipid interactions, five of the simulations have interaction on both helices, H1a PIP2, V1a PIP2, V2a PIP2, V1b PIP2, and V2b PIP2, and one lost structure, V1a PIP2, at the point of the possible stabilizing salt bridge interactions. The placement of the peptide in the membrane can be described by the hydrophobic residues on the α_6 helix that imbed deep into the membrane with the assistance of essential electrostatic residues (see the mutation section below) that guide the process. This can also be described with the many positively charged residues that are placed above the hydrophobic/hydrophilic interface and have greater selectivity for interacting with the POPS and PIP2 head group.

The α_7 helix is different from α_6 because the position is higher and some of the amino acid residues point down and lie above the membrane (R344 and R347). K336, K325, and R314 are important during the initial binding phase to guide the peptide into place and remain important

contributors after binding to keep the peptide on the membrane. Additionally, residues K315 and K334 orient upward and tilt to interact with the PIP2 lipids and POPS lipids. In general, the α_6 helix was deeper than the α_7 helix and the connection region of the peptide between the α_6 to α_7 helix is the deepest. The placement of these residues can be visualized with Figure S31-S34. One interesting residue to note is residue K315 which shows some variation in its placement. Figures S29, S30, and S35 show the different views and snapshots of the final states of the four full length simulations, and RMSD for HMMM shown in Figures S49 and S50.

In terms of *hypothesis 3,* the peptide bound orientations were measured again to see if the PIP2 lipids had any impact on the orientation, or more specifically the angle of approach. The PIP2 phosphates might be able to alter the angle of approach of the bound peptide and the orientation, but there was no data to support the validity of *hypothesis* 3. There was no difference in orientation between peptide bound on PIP2 and non-PIP2 membranes.

PIP2 Specific Interactions and Importance to Salt Bridges within Peptide

While testing *hypothesis 4* regarding the impact of PIP2 interactions, it was discovered that the PIP2 can compete for the same residues that create salt bridges between the two helices. An interesting discovery of the PIP2 simulations was identifying PIP2 and POPS lipid interactions with residue K315 compared to other residues. However, based on a T-test assuming unequal variance and a hypothesized mean difference of 0 for K315 interacting with anionic lipids compared to other residues, this was not found to be significant ($p=0.19$). This higher p-value is believed to be due to the heavy dependance of lipid sampling of the K315, and the fact that the PIP2 lipids were usually interacting with R344 and R347. These were observed to occur in a peptide state similar to that of the middle of the bottom panel of Figure 7 with the side chains tilted even more out to the sides. More sampling may be needed to fully explore lipid interaction with

the peptide due to slow PIP2 and POPS diffusion but this was beyond our general scope of the project.

Of the full-length lipid simulations, H1a PIP2 had many interactions closer than 4 Å over the entire full-length lipid simulation, between residues K315-D319, 43% of the time and between K334-E338, 33% of the time. The HMMM salt bridge data can be seen in Table S5, and the full-length data can be seen in Table S4. The position versus time for all amino acids in the simulations can be seen in Figures S36-S38. Figures S39 and S40 feature further conformational changes and K315 interacting with the POPS or PIP2 lipids. Figure S41 shows the specific conformational change on residue K315 only interacting with the PIP2 lipid. Figure S40 shows simulation V1b before the conformational change, and Figure S40 shows it after a conformational change with lipids to stabilize it. Finally, Figures S42 and S43 show the conformational change on residue K334 which was much less frequently observed and poorly sampled.

Residues Critical for Binding

While *hypothesis 1* asserts that certain residues play a key role, the interaction energy, hydrogen bonding, and salt bridges between the peptide and membrane are the key reasons for the roles residues play in binding and are investigated in this section. The energy per residue (Figure S44) indicates that the residues with lowest and attractive energy are at the ends of the peptide, and that the residues in the center such as Y318-T342 have higher energy. Figure S45 shows an unexpectedly high level of hydrogen bonding among R344 and R347 with the membrane because these residues only hover above the membrane surface and are not tightly bound to the membrane. Additionally, there are similarly high levels of salt bridges for the residues R344 and R347 in Figure S46. This indicates that these residues are important, but not as essential as the other residues.

Additionally, there were low levels of hydrogen bonds in the center of the peptide (V320-E340) and higher levels of hydrogen bonds among the remaining residues. K325 and K336 are an interesting exception to the rule of low hydrogen bonding in the center. These charged lysine residues are well oriented to interact with the membrane. The salt bridges between the membrane and the peptide indicate that the most frequent bridges occur with R314. The position of the deepest residue versus time is recorded in Figures S47 and S48 for the PIP2 simulations.

Effect of Mutating the Key Binding Residues

To verify the effect of the critical residues identified while researching *hypothesis 1*, mutations were performed. Two of the key binding residues (K325 and K336) were mutated to confirm their role in the binding process. In the wildtype simulations, these residues were pulled down underneath the membrane to the phosphate region, pulling with them some of the hydrophobic residues. Simulations with the K325D/K336D mutation caused the peptide not to bind to any extent onto the membrane. This is shown with *Movie* 7 of the supporting materials and image of the final state of the mutated peptide in Figure S51. This confirms that *hypothesis 1* is indeed valid and that K325 and K336 indeed play a role in the binding mechanism and keep the hydrophobic residues in contact with the hydrophobic core of the membrane.

Effect of Changing Force Field on Amino Acid-Lipid Interactions

The force field was changed adjusting pair-specific corrections to non-bonded interactions between the amine group of positively-charged amino acids and lipids (phosphate and/or carboxylate) known as CUFIX.[36] This change resulted in a drastic reduction in intermolecular interactions, based on simulations started from the end of the full length simulations and run for an additional 150 ns with CUFIX. The side-by-side comparison for hydrogen bonds can be found

in Figure S16 and S45; while the salt bridges are shown in Figure S17 and S46. The other factor is the interaction energy per residue, which is higher because of weaker electrostatic interactions. The CUFIX force field provides more of a balance between electrostatic and hydrophobic interactions, where the main reduction in interaction energy comes from the electrostatic contribution (Table 1).

Table 1. Demonstrates that there is a significant decrease in the total energy when switching to the CUFIX force field. The most stable binding was H1a PIP2 and V1b PIP2 where the PIP2 lipids are located on either side, the most stable of the non-PIP2 simulations is H2a.

Interaction Energy:	Total (kcal/mol)	van der Waals (kcal/mol)	Electrostatic (kcal/mol)
H1a	-287.0 ± 38.8	-87.9 ± 29.4	-140.8 ± 38.4
H2a	-358.7 ± 44.7	-87.4 ± 27.0	-184.1 ± 62.1
H1b	-351.7 ± 50.3	-100.2 ± 29.0	-201.9 ± 58.2
H2b	-288.8 ± 46.3	-85.8 ± 15.2	-186.9 ± 32.6
H1a PIP2	-425.0 ± 33.0	-94.3 ± 19.3	-246.5 ± 55.7
V2a PIP2	-331.7 ± 33.1	-79.3 ± 13.7	219.2 ± 44.8
V1b PIP2	-405.4 ± 51.0	-100.4 ± 25.3	-256.9 ± 65.3
V2b PIP2	-374.1 ± 53.1	-50.1 ± 26.0	-204.0 ± 71.9
H1a CUFIX	-155.3 ± 36.4	-74.9 ± 21.6	-49.3 ± 21.9
H2a CUFIX	-221.4 ± 40.9	-101.0 ± 23.6	85.0 ± 36.6
H1b CUFIX	-210.3 ± 36.2	-31.8 ± 45.0	-22.8 ± 37.3
H2b CUFIX	-151.6 ± 39.3	-70.5 ± 35.6	-51.6 ± 31.5
H1a PIP2 CUFIX	-206.8 ± 56.4	-86.1 ± 24.1	-85.8 ± 43.2
V2a PIP2 CUFIX	-171.7 ± 33.9	-67.0 ± 19.3	-68.9 ± 29.6
V1b PIP2 CUFIX	-210.1 ± 32.8	-99.9 ± 16.1	-90.7 ± 28.7
V2b PIP2 CUFIX	-225.6 ± 40.9	-79.4 ± 21.8	-92.8 ± 40.23

An important aspect of the PIP2 bound simulations is that the interaction energy was lower in the trials where the peptide bound directly on top of the PIP2 lipids. This occurred in trials V2a PIP2 and V2b PIP2 indicating that there is an energetic penalty if the peptide binds on top of the PIP2 lipids because the peptide is not as deeply bound. It is important to note here that V2b PIP2 CUFIX was not on top of lipids, the lipids moved out from under it. When the membrane is too highly enriched in PIP2 lipids, the peptide does not bind as deep, while when there is just the right amount, the peptide binds with PIP2 on the sides giving it a deeper placement than it would have without the PIP2 lipids.

The results of the total binding energy indicate that the standard force field has an average value of -352.8±49.7 kcal/mol, and the CUFIX has a value of -194.1±29.8 kcal/mol, and no

correlation between the angle of approach. This data shows that the PIP2 simulations were clearly lower energy than the non-PIP2 simulations. Specifically, the interaction energy for the non-PIP systems was -321.6 kcal/mol and -384.1 kcal/mol for those with PIP. However, with CUFIX the difference is smaller at -184.7 kcal/mol non-PIP2 and -203.6 kcal/mol for PIP. There was a weak statistical significance in the PIP2 vs. non-PIP2 membranes in the original force field ($p=0.068$) based on a T-test assuming unequal variance and a hypothesized difference of 0, but almost no statistical difference using the same hypothesis test in the CUFIX ($p=0.42$) indicating that this could be evidence of the overlapping roles of Osh proteins.[10] The PIP2 lipid membrane is capable of the lowest energy, but the peptide can achieve a similar binding energy on the non-PIP2 membrane.

On the other hand, there was evidence that certain amino acid residues were selective for PIP2 and POPS lipids and were out of reach of the main lipid POPC. These residues include K315, K334, R344, and R347. Of these the sum of the interaction energy of residues R344 and R347 is statistically significantly higher, ($p=0.018$) using a T-test assuming unequal variance and a hypothesized difference of 0, under the standard force field conditions, and has even higher significance using the same statistical test under the CUFIX conditions, ($p<10^{-5}$) with PIP2 lipids compared to non-PIP2 simulations with the same force field. The other two amino acids were not sampled as much because most the PIP2 lipids were interacting in different areas of the peptide neither of these was as statistically significant in the CUFIX force field, but they still selectively interacted with POPS and PIP2 head group over the O13 and O14 atoms that are deeper in the membrane. It is interesting that the only exceptions to the high selectivity are the amino acids that were mutated and found to prevent any level of binding which makes sense that these residues salt bridge with the deeper oxygen atoms. This is further evidence to support *hypothesis 1*. Figure 9

shows the relative selectivity of the different positively charged amino acid residues and shows that all amino acids have selectivity above 0.5 for both original force field and CUFIX force field except R314, K325, and K336. This is interesting because these are the amino acids that were identified to be critical to the binding process. Although residues K325 and K336 are the most selective for the O13 and O14 (deeper charged oxygens), residue R314 has a higher overall number of salt bridges (Figure 9B). The pie charts suggest that from this high level of perspective the force field does not perturb the overall fractions that each amino acid contributes, but instead plays more of a role in scaling the total number of interactions that occur.

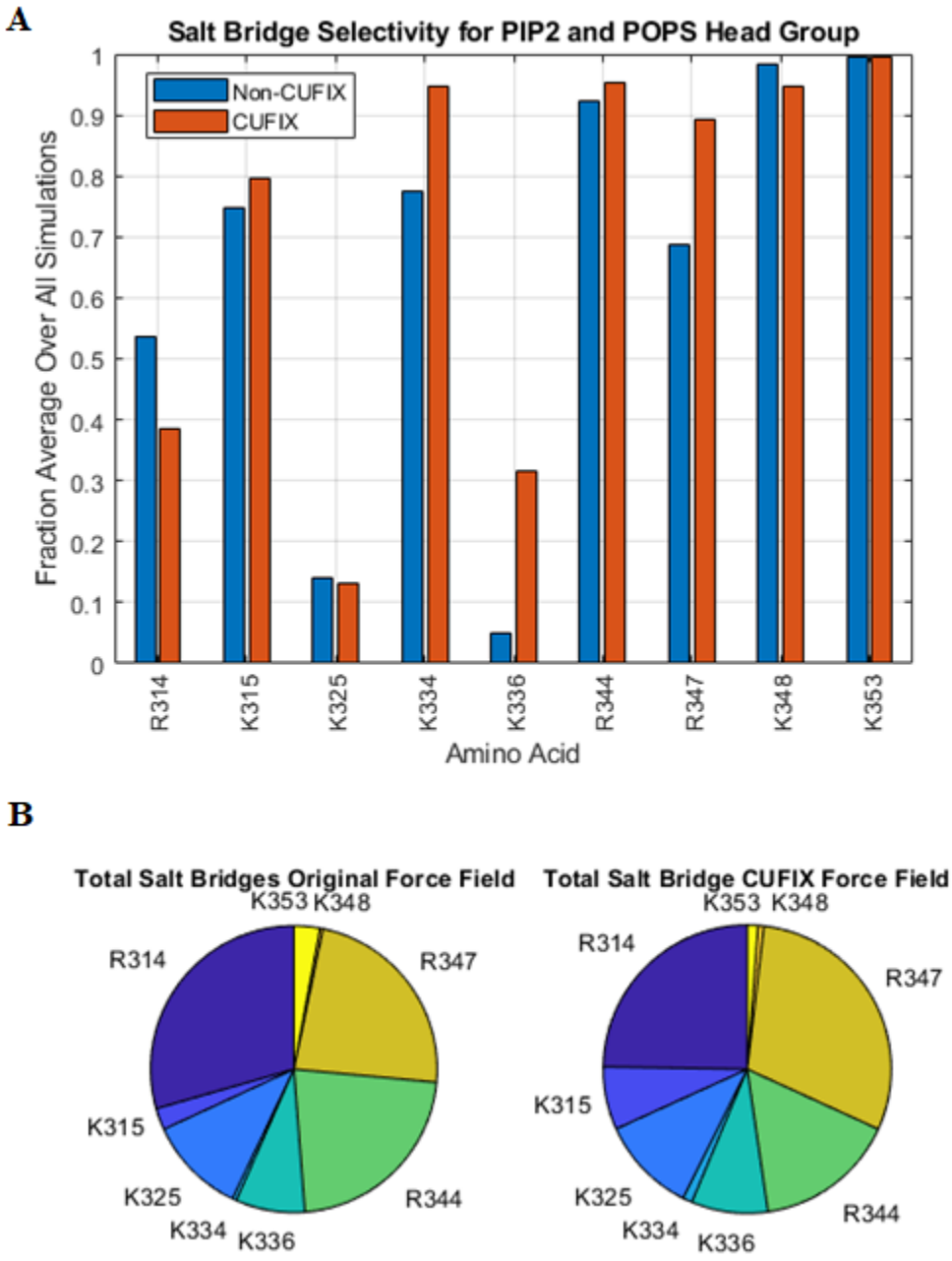

Figure 9) A. The selectivity of the different amino acids for the PIP2 and POPS head group, i.e., the fraction that is not interacting with the O13 and O14 (Figure 3) that are deeper in the bilayer. The results show that all of these amino acid residues are selective except for R314, K325 and K336 which are believed to play a role in guiding the insertion of the hydrophobic core of the peptide which is consistent with the low selectivity indicating more frequent salt bridges with the

deeper oxygen atoms. **B.** Pie chart of total salt bridges that notes while residues K348 and K353 have high selectivity, these have fewer overall salt bridges compared to other cationic amino acids.

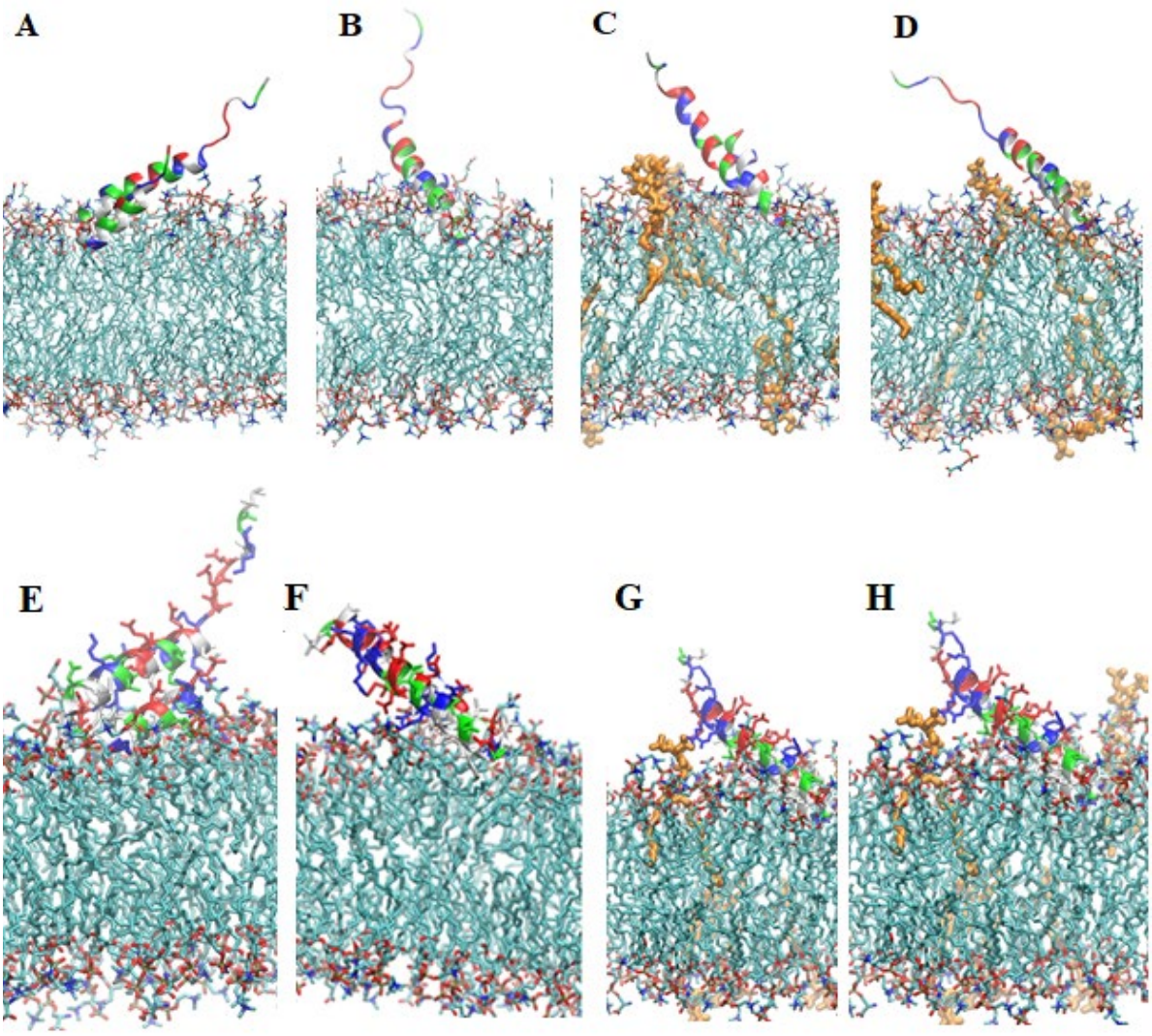

Figure 10) Images of the final bound states of the Osh α_6-α_7 helices **A** is H1a, **B** is H2a, **C** H1a PIP, and **D** is V2a PIP, **E** H1b, **F** H2b, **G** V1b, and **H** V2b.

Salt bridge interactions were found to promote the stability of tertiary structure of Osh4's α_6-α_7 peptide. There were salt bridge interactions between residues D319-K315, K315-E338, and E338-K334, as shown in Figures S19-S21 and S36-S38. Although the salt bridges were not always

present, they were still observed to exist for some of the time and therefore play some role in the stability of the peptide. In the case of H1a, the CUFIX simulations relaxed the peptide-peptide interactions increasing the number of conformations that residues K315 and K334 could adopt. For example, in the original force field the peptide-peptide interactions existed, but as soon as the force field was changed to CUFIX the salt bridge spanning across the two helices was broken. In other cases, it may have helped to speed up the diffusional process of lipids that were already interacting with the peptide.

Conclusions:

Of the four *hypotheses* that were probed in this work there were two that were confirmed to be true. *Hypothesis 1.,* Certain residues play a key role in the binding process; this was confirmed initially by observation, then verified by our peptide-membrane interaction analysis, and later by mutating two of the three proposed important residues to find that the peptide had severely reduced binding capacity. *Hypothesis 2.*, The mechanism of peptide binding is related to the angle of helical approach; this was proven to be invalid since there were a wide range of angles for both PIP2 and non-PIP2 trials. *Hypothesis 3.,* Peptide bound orientation differs in membranes with and without PIP2; there was no data supporting the hypothesis that the orientation of the peptide was affected by the presence of PIP2 lipids, because the angle of approach was not significantly altered. *Hypothesis 4.,*. Salt-bridge interactions between the two helices stabilize the membrane binding structure; this was found to be partially valid at least in the original C36/C36m force field, and there are indications of the same for the CUFIX force field as well.

Understanding the way in which peptides bind is an important first step in assessing its overall mechanism of action. Osh4's α_6-α_7 domain was able to bind to membranes with three critical amino acids including R314, K325, and K336 yielding strong membrane binding causing

insertion of much of the hydrophobic amino acids beneath the lipid head group. Salt bridges between the two helices stabilize the membrane binding sections K315-E338, as well as other salt bridges on the same helix K315-D319 and K334-E338 were observed. However, some of these salt bridge pairs destabilized in some simulations, but only one of the 20 total simulations caused drastic unfolding.

From past experimental work, it is known that Osh4 has a preference for PIP2 lipids, and that the protein will preferentially transport PI(4)P over other lipids types and the PI(4,5)P lipid accelerated transport of sterol.[18] Our simulation results demonstrate that signaling PIP2 lipids play a role in offering additional stability to the Osh α_6-α_7 domain. This supports the idea that PIP2 lipids signal lipid transport by stabilizing this binding domain. Specifically, our results indicate K315, K334, R344, and R347 are important residues for interactions with the PIP2 and POPS lipids, but not essential for function. In addition, our double mutational analysis of the wildtype to K325D/K336D shows that the peptide had no binding with the removal of the positively-charged lysine (see the video in the supporting materials *Movie* 7). This confirms that these amino acid residues are positioned to interact specifically with the deeper oxygen atoms that are shared among all the simulated lipids. There is experimental evidence indicating that PIP2 lipids speed up the lipid transfer process, and it was hypothesized that it was caused by increasing the dwell time on the liposome surface. [13, 17] However, our interaction energy results indicate that the peptide can be stable in membranes without PIP2 lipids and harness similar binding energies compared to PIP2 membranes. This is in line with the idea that the Osh proteins have overlapping roles since the α_6-α_7 peptide was capable of a similar binding energy and structure with and without any PIP2 lipids. Specific details on the free energy of binding in varied lipid environment will require enhanced sampling and replicas due to slow lipid diffusion and was beyond the scope of this work.

The current work shows that in addition to the ALPS motif, the α_6-α_7 helices are another membrane binding motif of Osh4.[28, 45] Future work will be done to simulate other parts of the Osh4 protein such as the ALPS section to learn more about how it can sense lipid packing. This work will guide new simulations of the full-length Osh4 that membrane binding will undoubtably be influenced by the β-crease,[46] but we will be probing how the α_6-α_7 helices simultaneously bind to membranes with the β-crease that might occur during binding events that consist of two opposing membranes.

Acknowledgements:

All simulations ran on the Extreme Science and Engineering Discovery Environment (XSEDE) supercomputer by grant number MCB-100139. Analysis of data was performed on the University of Maryland's Deeptought2 which is maintained by the Division of Information Technology. This research is supported by the NSF grant MCB-1951425.

Supporting Information:

The supporting materials has several different kinds of information including data figures, images of simulations, movies, and tables, and it is organized by non-PIP2 and full length first, PIP2 second, and the mutations last. To start the supporting materials off there are two tables one showing the distance between the main phosphate and the peptide center of mass, for all the simulation orientations. Second is a table showing the details of the peptide binding including the time of binding, minimum position or maximum penetration, and the center of mass relative to the bilayer phosphate. Then there are several data figures S1-S2 shows the deepest amino acid residue COM over time S3-S4 shows the RMSD of the simulations, and S5-10 shows the different angles

measured over time. Figures S11-S12 show the final bound states of the HMMM simulations, and S13-S14 show the RMSD of the full-length simulation. Figures S15-S17 show the interaction energy per residue, hydrogen bonds per residue and salt bridges per residue. Figure S18 shows the accessibility of residue K315 to hydrogen bonding with POPS lipids under the correct conditions, and figures S19-S21 show the distance between the different residues that form peptide-peptide salt bridges. Table S3-S4 shows the exact frequency of salt bridge formation as a fraction of 1 being 100% of the time. Figures S22-S25 show the placement graphs that are useful for seeing the position of all the amino acids over time and shows that there is some variation in the residue K315. Figure S26 shows snapshots of the peptide binding with PIP2 lipids around it, and S27 and S28 show the final bound HMMM sates of the PIP2 trials. Figure S29 and S30 show the final bound states of the PIP2 simulations, and Figure S31-S34 shows the placement graphs of PIP2 simulations with an additional image of final bound states in figure S35. Figures S36-S38 show the salt bridges for the PIP2 simulations with table S5 showing the salt bridge frequency as a fraction of 1. Figures S39-S43 show the different conformations that appear to be stabilized by PIP2 and POPS salt bridges interrupting the peptide-peptide salt bridges. Figures S44-S46 show the interaction energy per residue, hydrogen bonding per residue, and the salt bridges per residue. Then Figures S47-S48 show the position vs time of the COM of the deepest amino acid residue vs time, while Figures S49-S50 show the RMSD of all the PIP2 simulations. Finally there is a final image Figure S51 showing the final state of the mutated peptide showing that no binding took place.

References:

1. Lev, S., Non-vesicular lipid transport by lipid-transfer proteins and beyond. *Nature Reviews Molecular Cell Biology* **2010,** *11* (10), 739-750.
2. Fairn, G. D.; McMaster, C. R., Emerging roles of the oxysterol-binding protein family in metabolism, transport, and signaling. *Cellular and Molecular Life Sciences* **2008,** *65* (2), 228-236.
3. De Matteis, M. A.; Di Campli, A.; D'Angelo, G., Lipid-transfer proteins in membrane trafficking at the Golgi complex. *Biochimica et Biophysica Acta (BBA) - Molecular and Cell Biology of Lipids* **2007,** *1771* (6), 761-768.
4. Cockcroft, S., Mammalian phosphatidylinositol transfer proteins: emerging roles in signal transduction and vesicular traffic. *Chemistry and Physics of Lipids* **1999,** *98* (1), 23-33.
5. Holthuis, J. C. M.; Levine, T. P., Lipid traffic: floppy drives and a superhighway. *Nature Reviews Molecular Cell Biology* **2005,** *6* (3), 209-220.
6. Levine, T., Short-range intracellular trafficking of small molecules across endoplasmic reticulum junctions. *Trends in Cell Biology* **2004,** *14* (9), 483-490.
7. Kawano, M.; Kumagai, K.; Nishijima, M.; Hanada, K., Efficient Trafficking of Ceramide from the Endoplasmic Reticulum to the Golgi Apparatus Requires a VAMP-associated Protein-interacting FFAT Motif of CERT*. *Journal of Biological Chemistry* **2006,** *281* (40), 30279-30288.
8. Funato, K.; Riezman, H., Vesicular and nonvesicular transport of ceramide from ER to the Golgi apparatus in yeast. *The Journal of Cell Biology* **2001,** *155* (6), 949-960.
9. Hanada, K., Discovery of the molecular machinery CERT for endoplasmic reticulum-to-Golgi trafficking of ceramide. *Molecular and Cellular Biochemistry* **2006,** *286* (1), 23-31.
10. Im, Y. J.; Raychaudhuri, S.; Prinz, W. A.; Hurley, J. H., Structural mechanism for sterol sensing and transport by OSBP-related proteins. *Nature* **2005,** *437* (7055), 154-158.
11. Schulz, T. A.; Prinz, W. A., Sterol transport in yeast and the oxysterol binding protein homologue (OSH) family. *BBA - Molecular and Cell Biology of Lipids* **2007,** *1771* (6), 769-780.
12. Singh, R. P.; Brooks, B. R.; Klauda, J. B., Binding and release of cholesterol in the Osh4 protein of yeast. *Proteins: Structure, Function, and Bioinformatics* **2009,** *75* (2), 468-477.
13. Schulz, T. A.; Choi, M.-G.; Raychaudhuri, S.; Mears, J. A.; Ghirlando, R.; Hinshaw, J. E.; Prinz, W. A., Lipid-regulated sterol transfer between closely apposed membranes by oxysterol-binding protein homologues. *The Journal of Cell Biology* **2009,** *187* (6), 889-903.
14. Lemmon, M. A., Pleckstrin homology (PH) domains and phosphoinositides. *Biochemical Society Symposium* **2007,** *74*, 81-93.
15. Drin, G.; Jf, C.; R, G.; T, B.; Tu, S.; Antonny, B., A general amphipathic alpha-helical motif for sensing membrane curvature. *Nature Structural and Molecular Biology* **2007,** (1545-9993 (Print)).
16. Raychaudhuri, S.; Im, Y. J.; Hurley, J. H.; Prinz, W. A., Nonvesicular sterol movement from plasma membrane to ER requires oxysterol-binding protein–related proteins and phosphoinositides. *The Journal of Cell Biology* **2006,** *173* (1), 107.
17. Li, X.; Rivas, M. P.; Fang, M.; Marchena, J.; Mehrotra, B.; Chaudhary, A.; Feng, L.; Prestwich, G. D.; Bankaitis, V. A., Analysis of oxysterol binding protein homologue Kes1p function in regulation of Sec14p-dependent protein transport from the yeast Golgi complex. *The Journal of Cell Biology* **2002,** *157* (1), 63.
18. de Saint-Jean, M.; Delfosse, V.; Douguet, D.; Chicanne, G.; Payrastre, B.; Bourguet, W.; Antonny, B.; Drin, G., Osh4p exchanges sterols for phosphatidylinositol 4-phosphate between lipid bilayers. *The Journal of Cell Biology* **2011,** *195* (6), 965.
19. MarvinSketch. https://chemaxon.com/: 2020.
20. Jo, S.; Kim, T.; Iyer, V. G.; Im, W., CHARMM-GUI: A web-based graphical user interface for CHARMM. *Journal of Computational Chemistry* **2008,** *29* (11), 1859-1865.
21. Jo, S.; Lim, J. B.; Klauda, J. B.; Im, W., CHARMM-GUI Membrane Builder for Mixed Bilayers and Its Application to Yeast Membranes. *Biophysical Journal* **2009,** *97* (1), 50-58.

22. Jo, S.; Kim, T.; Im, W., Automated Builder and Database of Protein/Membrane Complexes for Molecular Dynamics Simulations. *PLOS ONE* **2007,** *2* (9), e880.
23. Qi, Y.; Cheng, X.; Lee, J.; Vermaas, J. V.; Pogorelov, T. V.; Tajkhorshid, E.; Park, S.; Klauda, J. B.; Im, W., CHARMM-GUI HMMM Builder for Membrane Simulations with the Highly Mobile Membrane-Mimetic Model. (1542-0086 (Electronic)).
24. Lee, J.; Patel, D. S.; Ståhle, J.; Park, S.-J.; Kern, N. R.; Kim, S.; Lee, J.; Cheng, X.; Valvano, M. A.; Holst, O.; Knirel, Y. A.; Qi, Y.; Jo, S.; Klauda, J. B.; Widmalm, G.; Im, W., CHARMM-GUI Membrane Builder for Complex Biological Membrane Simulations with Glycolipids and Lipoglycans. *Journal of Chemical Theory and Computation* **2019,** *15* (1), 775-786.
25. Wu, E. L.; Cheng, X.; Jo, S.; Rui, H.; Song, K. C.; Dávila-Contreras, E. M.; Qi, Y.; Lee, J.; Monje-Galvan, V.; Venable, R. M.; Klauda, J. B.; Im, W., CHARMM-GUI Membrane Builder toward realistic biological membrane simulations. *J Comput Chem* **2014,** *35* (27), 1997-2004.
26. Ohkubo, Y. Z.; Tv, P.; Mj, A.; Ga, C.; Tajkhorshid, E., Accelerating membrane insertion of peripheral proteins with a novel membrane mimetic model. *Biophys, J.* (1542-0086 (Electronic)).
27. Jorgensen, W. L.; Chandrasekhar, J.; Madura, J. D.; Impey, R. W.; Klein, M. L., Comparison of simple potential functions for simulating liquid water. *The Journal of Chemical Physics* **1983,** *79* (2), 926-935.
28. Wildermuth, K. D.; Monje-Galvan, V.; Warburton, L. M.; Klauda, J. B., Effect of Membrane Lipid Packing on Stable Binding of the ALPS Peptide. *Journal of Chemical Theory and Computation* **2019,** *15* (2), 1418-1429.
29. Brooks, B. R.; Brooks Iii, C. L.; Mackerell Jr, A. D.; Nilsson, L.; Petrella, R. J.; Roux, B.; Won, Y.; Archontis, G.; Bartels, C.; Boresch, S.; Caflisch, A.; Caves, L.; Cui, Q.; Dinner, A. R.; Feig, M.; Fischer, S.; Gao, J.; Hodoscek, M.; Im, W.; Kuczera, K.; Lazaridis, T.; Ma, J.; Ovchinnikov, V.; Paci, E.; Pastor, R. W.; Post, C. B.; Pu, J. Z.; Schaefer, M.; Tidor, B.; Venable, R. M.; Woodcock, H. L.; Wu, X.; Yang, W.; York, D. M.; Karplus, M., CHARMM: The biomolecular simulation program. *Journal of Computational Chemistry* **2009,** *30* (10), 1545-1614.
30. Lee, J.; Cheng, X.; Swails, J. M.; Yeom, M. S.; Eastman, P. K.; Lemkul, J. A.; Wei, S.; Buckner, J.; Jeong, J. C.; Qi, Y.; Jo, S.; Pande, V. S.; Case, D. A.; Brooks, C. L.; MacKerell, A. D.; Klauda, J. B.; Im, W., CHARMM-GUI Input Generator for NAMD, GROMACS, AMBER, OpenMM, and CHARMM/OpenMM Simulations Using the CHARMM36 Additive Force Field. *Journal of Chemical Theory and Computation* **2016,** *12* (1), 405-413.
31. Ryckaert, J.-P.; Ciccotti, G.; Berendsen, H. J. C., Numerical integration of the cartesian equations of motion of a system with constraints: molecular dynamics of n-alkanes. *Journal of Computational Physics* **1977,** *23* (3), 327-341.
32. Klauda, J. B.; Venable, R. M.; Freites, J. A.; O'Connor, J. W.; Tobias, D. J.; Mondragon-Ramirez, C.; Vorobyov, I.; MacKerell, A. D.; Pastor, R. W., Update of the CHARMM All-Atom Additive Force Field for Lipids: Validation on Six Lipid Types. *The Journal of Physical Chemistry B* **2010,** *114* (23), 7830-7843.
33. Li, Z.; Venable, R. M.; Rogers, L. A.; Murray, D.; Pastor, R. W., Molecular Dynamics Simulations of PIP2 and PIP3 in Lipid Bilayers: Determination of Ring Orientation, and the Effects of Surface Roughness on a Poisson-Boltzmann Description. *Biophysical Journal* **2009,** *97* (1), 155-163.
34. Best, R. B.; Zhu, X.; Shim, J.; Lopes, P. E. M.; Mittal, J.; Feig, M.; MacKerell, A. D., Optimization of the Additive CHARMM All-Atom Protein Force Field Targeting Improved Sampling of the Backbone ϕ, ψ and Side-Chain $\chi1$ and $\chi2$ Dihedral Angles. *Journal of Chemical Theory and Computation* **2012,** *8* (9), 3257-3273.
35. Huang, J.; Rauscher, S.; Nawrocki, G.; Ran, T.; Feig, M.; de Groot, B. L.; Grubmüller, H.; MacKerell, A. D. J., CHARMM36m: an improved force field for folded and intrinsically disordered proteins. *Nat, Methods* (1548-7105 (Electronic)).
36. Yoo, J.; Aksimentiev, A., New tricks for old dogs: improving the accuracy of biomolecular force fields by pair-specific corrections to non-bonded interactions. *Physical Chemistry Chemical Physics* **2018,** *20* (13), 8432-8449.

37. Steinbach, P. J.; Brooks, B. R., New spherical-cutoff methods for long-range forces in macromolecular simulation. *Journal of Computational Chemistry* **1994,** *15* (7), 667-683.
38. Hoover, W. G., Canonical dynamics: Equilibrium phase-space distributions. *Physical Review A* **1985,** *31* (3), 1695-1697.
39. Darden, T.; York, D.; Pedersen, L., Particle mesh Ewald: An N·log(N) method for Ewald sums in large systems. *The Journal of Chemical Physics* **1993,** *98* (12), 10089-10092.
40. Phillips, J. C.; Braun, R.; Wang, W.; Gumbart, J.; Tajkhorshid, E.; Villa, E.; Chipot, C.; Skeel, R. D.; Kalé, L.; Schulten, K., Scalable molecular dynamics with NAMD. *Journal of Computational Chemistry* **2005,** *26* (16), 1781-1802.
41. Feller, S. E.; Zhang, Y.; Pastor, R. W.; Brooks, B. R., Constant pressure molecular dynamics simulation: The Langevin piston method. *The Journal of Chemical Physics* **1995,** *103* (11), 4613-4621.
42. Martyna, G. J.; Tobias, D. J.; Klein, M. L., Constant pressure molecular dynamics algorithms. *The Journal of Chemical Physics* **1994,** *101* (5), 4177-4189.
43. Humphrey, W.; Dalke, A.; Schulten, K., VMD: Visual molecular dynamics. *Journal of Molecular Graphics* **1996,** *14* (1), 33-38.
44. Stone, J., An Efficient Library for Parallel Ray Tracing and Animation. Computer Science Department, University of Missouri-Rolla: 1998.
45. Monje-Galvan, V.; Klauda, J. B., Preferred Binding Mechanism of Osh4's Amphipathic Lipid-Packing Sensor Motif, Insights from Molecular Dynamics. *The Journal of Physical Chemistry B* **2018,** *122* (42), 9713-9723.
46. Monje-Galvan, V.; Klauda, J. B., Peripheral membrane proteins: Tying the knot between experiment and computation. *Biochimica et Biophysica Acta (BBA) - Biomembranes* **2016,** *1858* (7, Part B), 1584-1593.

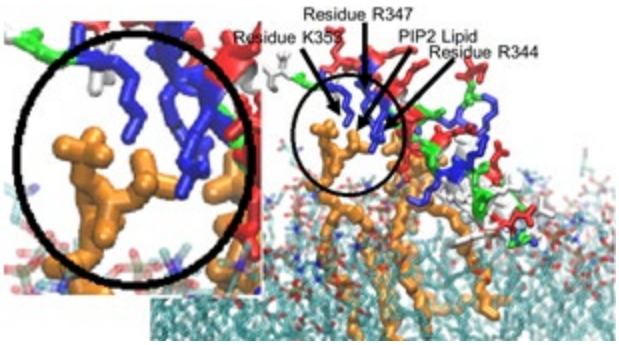

For Table of Contents Only